High resolution infrared and Raman spectra of 13C12CD2: The CD stretching fundamentals and associated combination and hot bands

G. Di Lonardo, L. Fusina, E. Canè, F. Tamassia, R. Z. Martínez, and D. Bermejo

Citation: The Journal of Chemical Physics **143**, 094302 (2015); doi: 10.1063/1.4929723

View online: http://dx.doi.org/10.1063/1.4929723

View Table of Contents: http://scitation.aip.org/content/aip/journal/jcp/143/9?ver=pdfcov

Published by the AIP Publishing

High resolution infrared and Raman spectra of $^{13}C^{12}CD_2$: The CD stretching fundamentals and associated combination and hot bands

G. Di Lonardo,[1] L. Fusina,[1,a)] E. Canè,[1] F. Tamassia,[1] R. Z. Martínez,[2] and D. Bermejo[2]
[1]*Dipartimento di Chimica Industriale "Toso Montanari," Università di Bologna, Viale Risorgimento 4, I-40136 Bologna, Italy*
[2]*Instituto de Estructura de la Materia, IEM-CSIC, Serrano 123, 28006 Madrid, Spain*

(Received 16 April 2015; accepted 4 August 2015; published online 3 September 2015)

Infrared and Raman spectra of mono ^{13}C fully deuterated acetylene, $^{13}C^{12}CD_2$, have been recorded and analysed to obtain detailed information on the C—D stretching fundamentals and associated combination, overtone, and hot bands. Infrared spectra were recorded at an instrumental resolution ranging between 0.006 and 0.01 cm^{-1} in the region 1800–7800 cm^{-1}. Sixty new bands involving the ν_1 and ν_3 C—D stretching modes also associated with the ν_4 and ν_5 bending vibrations have been observed and analysed. In total, 5881 transitions have been assigned in the investigated spectral region. In addition, the Q branch of the ν_1 fundamental was recorded using inverse Raman spectroscopy, with an instrumental resolution of about 0.003 cm^{-1}. The transitions relative to each stretching mode, i.e., the fundamental band, its first overtone, and associated hot and combination bands involving bending states with $\upsilon_4 + \upsilon_5$ up to 2 were fitted simultaneously. The usual Hamiltonian appropriate to a linear molecule, including vibration and rotation *l*-type and the Darling–Dennison interaction between $\upsilon_4 = 2$ and $\upsilon_5 = 2$ levels associated with the stretching states, was adopted for the analysis. The standard deviation for each global fit is $\leq 0.0004\,cm^{-1}$, of the same order of magnitude of the measurement precision. Slightly improved parameters for the bending and the ν_2 manifold have been also determined. Precise values of spectroscopic parameters deperturbed from the resonance interactions have been obtained. They provide quantitative information on the anharmonic character of the potential energy surface, which can be useful, in addition to those reported in the literature, for the determination of a general anharmonic force field for the molecule. Finally, the obtained values of the Darling–Dennison constants can be valuable for understanding energy flows between independent vibrations. © *2015 AIP Publishing LLC.* [http://dx.doi.org/10.1063/1.4929723]

I. INTRODUCTION

Owing to its theoretical, experimental, atmospheric,[1] and astrophysical[2,3] importance, acetylene and its isotopically substituted species have been the subject of extensive spectroscopic investigations. A comprehensive review on theoretical background and research trends of the high-resolution infrared (IR) spectroscopy of acetylene has been recently published.[4]

The determination of the isotopic ratio of various elements in different regions of the universe can provide useful information to understand the evolution of astrophysical media. In spite of the low cosmic abundance of deuterium, single, doubly, and even triply deuterated molecules have been detected in interstellar space. Deuterated acetylenes can provide information on the H/D ratio in various regions of the interstellar medium and in planetary atmospheres. C_2HD has already been detected in Titan's atmosphere[5] and various perdeuterated molecules have been observed in many different sources (see Ref. 6 and references therein), but no observation of $^{12}C_2D_2$ has been reported so far. In the event that $^{12}C_2D_2$ would be identified, the presence of $^{13}C^{12}CD_2$ could be searched for to yield information on the $^{13}C/^{12}C$ isotopic ratio.

The knowledge of precise spectroscopic information on the vibrational states up to high energy for all stable isotopologues of acetylene could also stimulate the determination of a mass independent anharmonic force field for the molecule based on experiments. The results of this study could be compared to those obtained from high level *ab initio* calculations.

In recent years, high resolution IR and Raman spectroscopies have provided accurate characterization of the bending modes with $\upsilon_{tot} = \upsilon_4 + \upsilon_5$ up to 3[7] and of the ν_2 C≡C stretching mode[8,9] for $^{13}C^{12}CD_2$. In addition, the $2\nu_1 + 2\nu_2 + \nu_3 \leftarrow$ GS (Ground State) and $\nu_1 + \nu_2 + 3\nu_3 \leftarrow$ GS bands were investigated in the 10 000–12 000 cm^{-1} region using the Intracavity Laser Absorption Spectroscopy experimental technique.[10] More recently, the $\nu_1 + \nu_2 + \nu_3 \leftarrow$ GS and associated hot bands from ν_4 and ν_5 and $2\nu_1 + \nu_4 + \nu_5 \leftarrow$ GS were recorded in the 6130–6800 cm^{-1} region using a Femto-FT-CEAS (Fourier transform cavity enhanced absorption spectroscopy) apparatus.[11] An early study by Ghersetti *et al.*[12] reported the spectra of the ν_3, $\nu_3 + \nu_4$ and $\nu_3 + \nu_5$ bands at moderate resolution in a ^{13}C enriched sample of $^{12}C_2D_2$.

The vibrational assignments are provided in terms of the usual normal modes of vibration in acetylene, namely, the symmetric (ν_1) and antisymmetric (ν_3) C—D stretchings, the C≡C stretching (ν_2), the degenerate *trans* (ν_4) and *cis* (ν_5) bendings,

a)Author to whom correspondence should be addressed. Electronic mail: luciano.fusina@unibo.it

and the vibrational angular momentum quantum numbers l_4 and l_5. This will facilitate the comparison of the spectroscopic parameters for the various isotopologues.

The aim of the present investigation is to provide, for the first time, high quality spectroscopic data for the C—D stretching modes of this exotic isotopologue of the most important prototype of a four atom linear molecule, up to high energy. High resolution IR and Raman spectra of the bands involving the ν_1 and ν_3 modes, the first associated overtone, combination, and hot bands with ν_4 and ν_5 bending excitations have been recorded between 1800 and 7800 cm^{-1} and analysed.

All the transitions assigned to a given fundamental, overtones, and stretching-bending combinations were fitted together providing a set of accurately determined parameters. They include the vibration and rotation parameters, the l-type, and the $\upsilon_4 = 2/\upsilon_5 = 2$ Darling–Dennison (D–D) interaction constants. The last parameter represents the most important anharmonic resonance interaction between rovibrational levels in fully deuterated acetylenes. It can provide the path for the energy flow (intramolecular vibrational redistribution) between independent vibrational degrees of freedom of the molecule, particularly at high energies as illustrated by Jonas *et al.*[13] for $^{12}C_2H_2$. Since its effects on the energy pattern usually scale with increasing vibrational excitation, it is essential to determine its value at the fundamental levels with high accuracy, in order to precisely calculate the effects of the perturbation in the overtone region.

The results of the present investigation complete the characterization of all the vibration modes of the 10 stable isotopologues of acetylene.

The text is structured as follows. The experimental details and the description of the spectra are given on Sections II and III, respectively. The assignments, the theoretical model used in the analysis, and the fit procedures are reported in Sections IV and V. Section VI outlines the results and the conclusions are in Section VII.

II. EXPERIMENT

The sample of the $^{13}C^{12}CD_2$ molecule was synthesised as described in Ref. 14. The reaction sequence is

$$\left[Si(CH_3)_3\right]_2NLi \xrightarrow[2.\ CH_3CO_2D]{1.\ BrH_2^{13}C^{12}CH_2Br} D^{13}C^{12}CD + D^{13}C^{12}CH + H^{13}C^{12}CD + H^{13}C^{12}CH.$$

In particular, the precursor $BrH_2{}^{13}C^{12}CH_2Br$ was prepared starting from $^{13}CH_3^{12}CH_2OH$ as detailed in Ref. 8. Using a large amount of deuterating compound, the percentage of $^{13}C^{12}CD_2$ in the mixture rised to about 60% and only traces of $^{13}C^{12}CH_2$ were present. As usual, the presence in the sample of ^{13}C mono-substituted and partially deuterated ethylenes cannot be avoided.

The spectra were recorded between 1800 and 7800 cm^{-1} using a Bomen DA3.002 Fourier transform (FT) spectrometer in Bologna. In the region 1800–2300 cm^{-1}, a Globar source, a KBr beam splitter, and a high-sensitivity HgCdTe detector were used. In the 2300–7800 cm^{-1} interval, the same source and beam splitter were used, whereas the detector was an InSb type equipped with a $N_2(l)$ cooled filter which restricted the observation down to 2300 cm^{-1}. Above 4500 cm^{-1}, a quartz beam splitter was adopted. In both regions, the optical path was set equal to 0.16 or 10 m. Different pressure conditions, from 133.3 Pa to 1333.3 Pa, were adopted. The achieved resolution (full width at half maximum for isolated lines) ranged from 0.006 to about 0.016 cm^{-1}, depending on the sample pressure adopted and the Doppler width of the lines. Ro-vibration transitions of H_2O,[15,16] and CO_2,[17] applying the correction according to Ref. 18, were used to calibrate the spectra. The calibration deserved particular care in order to obtain consistent results from the analysis of bands observed in different spectral regions but reaching the same excited state. The wavenumber precision and accuracy is ca. 4×10^{-4} cm^{-1}.

A detailed description of the Raman experimental setup and wavenumber calibration can be found in Ref. 8. In the present case, the laser dyes have been changed to match the desired spectral region: a ~50% mixture of Rhodamine B and Rhodamine 101 in ethylene glycol has been used for the CW dye laser and an ethanol solution of DCM for the dye amplifier. The sample pressure was 1500 Pa at room temperature. Spectra were recorded six times and averaged in order to increase the signal to noise ratio. The achieved resolution was of 0.009 cm^{-1}.

III. DESCRIPTION OF THE SPECTRA

The IR spectrum of $^{13}C^{12}CD_2$ from 1800 to 7800 cm^{-1} is complicated by the presence of absorption lines due mainly to the partially deuterated species, $H^{13}C^{12}CD$ and $D^{13}C^{12}CH$, in the sample. The spectrum is dominated by the ν_3 fundamental band of the antisymmetric C—D stretching motion at 2432.08 cm^{-1}. Because of the absence of a centre of symmetry in the molecule, the ν_1 fundamental of the symmetric C—D stretching is also visible at 2679.27 cm^{-1}, but with low intensity. A large number of stretching-bending combination bands associated to these transitions could be detected in the IR spectrum. In total, 63 bands were assigned, 59 of which were newly observed.

A. The 1800–2200 cm^{-1} region

In this region, two weak perpendicular bands, the difference bands of the two C—D stretching vibrations, $\nu_3 \leftarrow \nu_4$ ($\Sigma^+ \leftarrow \Pi$) at 1927.11 cm^{-1}, see Fig. 1, $\nu_1 \leftarrow \nu_5$ ($\Sigma^+ \leftarrow \Pi$) at 2142.64 cm^{-1}, and the associated bands involving the bending modes are present, namely, $\nu_3 + \nu_4 \leftarrow 2\nu_4$ ($\Pi \leftarrow \Sigma^+$ and $\Pi \leftarrow \Delta$) at 1918.16 and 1918.66 cm^{-1}, $\nu_3 + \nu_5 \leftarrow \nu_4 + \nu_5$ ($\Pi \leftarrow \Sigma^+$) at 1928.50 cm^{-1}, $\nu_1 + \nu_4 \leftarrow \nu_4 + \nu_5$ ($\Pi \leftarrow \Sigma^+$) at 2134.64 cm^{-1}, and $\nu_1 + \nu_5 \leftarrow 2\nu_5$ ($\Pi \leftarrow \Sigma^+$ and $\Pi \leftarrow \Delta$) at 2139.44 and 2134.85 cm^{-1}, respectively.

B. The 2400–2500 cm^{-1} region

This region of the spectrum is dominated by the strong parallel $\nu_3 \leftarrow$ GS band ($\Sigma^+ \leftarrow \Sigma^+$) at 2432.08 cm^{-1}. A large number of hot bands can be observed in the same region, namely, $\nu_3 + \nu_4 \leftarrow \nu_4$ ($\Pi \leftarrow \Pi$) at 2426.42 cm^{-1}, $\nu_3 + \nu_5 \leftarrow \nu_5$ ($\Pi \leftarrow \Pi$) at 2427.05 cm^{-1}, and all the bands of the kind

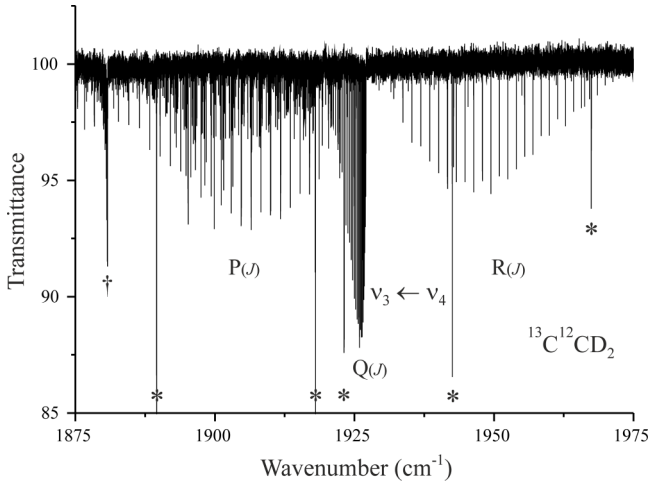

FIG. 1. Portion of the infrared spectrum of $^{13}C^{12}CD_2$ in the range 1875–1975 cm^{-1} showing the $\nu_3 \leftarrow \nu_4$ ($\Sigma^+ \leftarrow \Pi$) band. Q(J) and R(J) transitions are clearly visible whereas the P(J) lines overlap the R branch of the $\nu_7+\nu_8$ band of mono ^{13}C deuterated ethylene, whose Q branch is identified by a dagger. Lines marked by an asterisk belong to the ν_2 band of water. Experimental conditions: room temperature, pressure 1333.3 Pa, path length 0.16 m, and resolution 0.008 cm^{-1}.

$\nu_3 + (n\nu_4 + m\nu_5) \leftarrow (n\nu_4 + m\nu_5)$, where $n + m = 2$ and the two states in parenthesis are identical.

C. The 2600–2800 cm^{-1} region

This region of the spectrum contains the moderately weak parallel $\nu_1 \leftarrow$ GS band ($\Sigma^+ \leftarrow \Sigma^+$) at 2679.27 cm^{-1}, which is weakly allowed due to the lack of the centre of symmetry in the molecule. The Q branch of ν_1 can also be seen in the stimulated Raman spectrum under high resolution, thanks to the high sensitivity of the apparatus, see Fig. 2. The line identified by an asterisk in the figure corresponds to the O(2) transition, the first line of the $\Delta J = -2$ branch. It is worth noting that the width of this line is much larger than that of the Q(J) lines, where the pattern of Stark splitting generated by the intense electric field of the laser and shifting of the lower

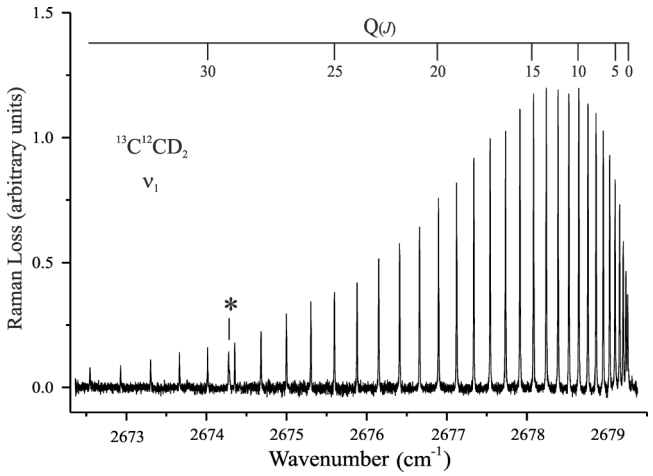

FIG. 2. Raman spectrum of the Q branch of the ν_1 band at room temperature, pressure 1550 Pa, and resolution 0.009 cm^{-1}. The line identified by an asterisk at 2674.3 cm^{-1} is the O(2) transition, the first line of the $\Delta J = -2$ branch.

and higher levels is very similar since $J' = J''$. All the hot bands of the kind described above for ν_3 are also present in the region of ν_1, with the exception of $\nu_1 + 2\nu_4 \leftarrow 2\nu_4$ ($\Sigma^+ \leftarrow \Sigma^+$ and $\Delta \leftarrow \Delta$), which are too weak to be seen in the spectrum. In addition, the $\nu_1 + \nu_4 \leftarrow \nu_5$ ($\Pi \leftarrow \Pi$) band is observed at 2633.19 cm^{-1}. The analogous $\nu_3 + \nu_4 \leftarrow \nu_5$ ($\Pi \leftarrow \Pi$) band has not been detected.

D. The 2800–3600 cm^{-1} region

Two bands of medium intensity are observed: $\nu_3 + \nu_4$ (Π) $\leftarrow$ GS, at 2931.39 cm^{-1} and $\nu_1 + \nu_5$ (Π) $\leftarrow$ GS, at 3207.73 cm^{-1}. Each band is accompanied by a few hot bands from both ν_4 and ν_5. The $\nu_1 + \nu_5$ (Π) state can also be characterised through the weak ($\Pi \leftarrow \Pi$) band from ν_4 at 2702.76 cm^{-1}. Other very weak bands are present in this region, namely, $\nu_3 + 2\nu_4$ (Σ^+ and $\Delta_{(e)}$) $\leftarrow$ GS at 3433.72 and 3433.42 cm^{-1}, respectively, and $\nu_3 + 2\nu_5$ (Σ^+) $\leftarrow$ GS at 3490.32 cm^{-1}. The $\nu_3 + 2\nu_4 \leftarrow$ GS, ($\Delta_{(e)} \leftarrow \Sigma^+$), band is a perturbation-allowed transition.

E. The 3600–5200 cm^{-1} region

Three bands are prominent in this region of the spectrum: the medium-weak $\nu_2 + \nu_3$ (Σ^+) $\leftarrow$ GS at 4167.47 cm^{-1}, the weak $2\nu_3(\Sigma^+) \leftarrow$ GS at 4834.46 cm^{-1}, and the strong $\nu_1 + \nu_3$ (Σ^+) $\leftarrow$ GS at 5064.17 cm^{-1}, see Fig. 3. The first and the last bands are accompanied by hot bands from ν_4 and ν_5. A rather weak band, namely, $\nu_2 + \nu_3 + 2\nu_4$ (Σ^+) $\leftarrow$ GS, is observed, at 5162.09 cm^{-1}.

F. The 5200–5900 cm^{-1} region

Four weak bands are present in this region: the parallel $2\nu_1$ (Σ^+) $\leftarrow$ GS at 5334.27 cm^{-1}, the perpendicular $2\nu_3 + \nu_5$ (Π) $\leftarrow$ GS at 5361.00 cm^{-1}, the very weak parallel $\nu_1 + \nu_2 + \nu_4 + \nu_5$ (Σ^+) $\leftarrow$ GS at 5418.42 cm^{-1}, and the perpendicular $2\nu_1 + \nu_5$ (Π) $\leftarrow$ GS at 5854.73 cm^{-1}.

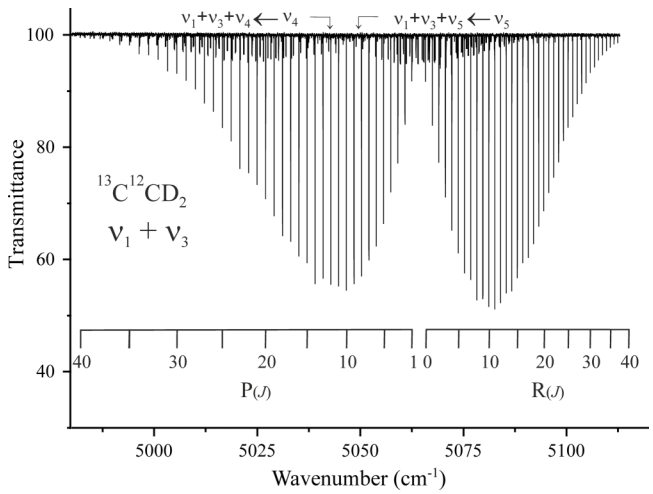

FIG. 3. Portion of the infrared spectrum of $^{13}C^{12}CD_2$ in the range 4980–5115 cm^{-1} showing the P and R branches of the $\nu_1+\nu_3 \leftarrow$ GS ($\Sigma^+ \leftarrow \Sigma^+$) band and of associated hot bands from ν_4 and ν_5. Experimental conditions: room temperature, pressure 1333.3 Pa, path length 0.16 m, and resolution 0.016 cm^{-1}.

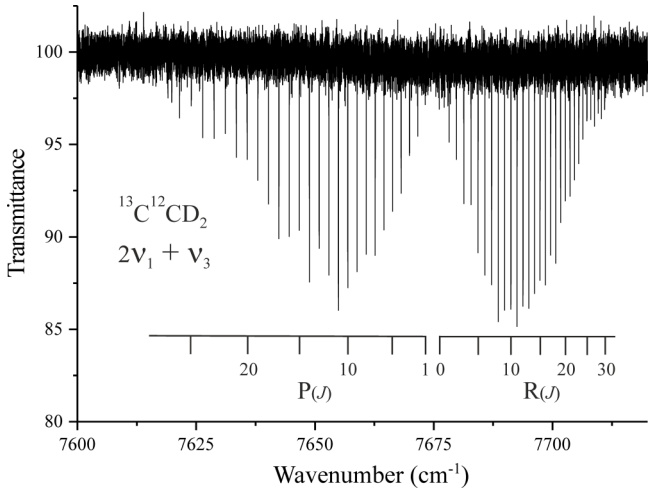

FIG. 4. Portion of the infrared spectrum of $^{13}C^{12}CD_2$ in the range 7600–7720 cm^{-1} showing the combination band $2\nu_1+\nu_3 \leftarrow$ GS ($\Sigma^+ \leftarrow \Sigma^+$). Experimental conditions: room temperature, pressure 378 Pa, path length 10 m, and resolution 0.023 cm^{-1}.

G. The 5900–7800 cm^{-1} region

Four out of six bands present in this region of the spectrum were already reported in a previous work,[11] $\nu_1 + \nu_2 + \nu_3$ (Σ^+) $\leftarrow$ GS at 6780.07 cm^{-1}, and the accompanying hot bands from ν_4 and ν_5 at 6755.60 cm^{-1} and 6768.14 cm^{-1}, respectively. The band $2\nu_1 + \nu_4 + \nu_5$ (Σ^+) $\leftarrow$ GS at 6324.45 cm^{-1} is too weak to be seen under the present experimental conditions. The two weak parallel remaining bands are $3\nu_3$ (Σ^+) $\leftarrow$ GS at 7207.16 cm^{-1} and $2\nu_1 + \nu_3$ (Σ^+) $\leftarrow$ GS at 7674.99 cm^{-1}, see Fig. 4.

IV. ASSIGNMENT

All the 60 bands analysed in the present study are collected in Table I, together with the symmetry of the vibrational states involved in the transition, the band centre, the observed range of J'' values for the various branches, the number of fitted and assigned lines, and the RMS error resulting from the simultaneous least squares analysis described below. In addition, bands reported in Refs. 10 and 11 are listed in Table I for completeness.

Lower state combination differences (LSCDs) calculated from the parameters reported in Table II, which were obtained as described below, were used to assign the J'' values of the transitions and to identify the lower vibrational state. The upper state of each transition was assigned comparing its term value with those reported for the other fully deuterated isotopologues, $^{12}C_2D_2$[19] and $^{13}C_2D_2$.[20–22] Once the identification of the upper state was achieved, we systematically searched transitions reaching it from different lower states.

The spectroscopic analysis of the assigned bands was accomplished in two steps. First, the transition wavenumbers for each band were fitted separately to effective upper state ro-vibrational parameters, to check the correctness of the assignments, and to extend the data set to higher J transitions. The effective Hamiltonian for a linear molecule, including the l-doubling energy contributions for transitions involving doubly degenerate states, was adopted for the analysis. The ro-vibrational term values are given by

$$T^0(\upsilon, J) = G_c^0(\upsilon) + B_\upsilon J(J+1) - D_\upsilon[J(J+1)]^2 + H_\upsilon[J(J+1)]^3 + \cdots \pm 1/2\left\{q_\upsilon\,[J(J+1)] + q_\upsilon^J[J(J+1)]^2 + q_\upsilon^{JJ}[J(J+1)]^3 + \cdots\right\}, \quad (1)$$

with the – and + signs related to the e and f levels, respectively, and the centre energy $G_c^0 = G_\upsilon^0 - B_\upsilon k^2 - D_\upsilon k^4$, where G_υ^0 is the pure vibrational term value defined in Eq. (3) and $k = l_4 + l_5$.

The band centre is defined as

$$\nu_C = G_{\upsilon'}^0 - B_{\upsilon'}k^2 - D_{\upsilon'}k^4 - (G_{\upsilon''}^0 - B_{\upsilon''}k^2 - D_{\upsilon''}k^4), \quad (2)$$

where $G_{\upsilon'}^0$ and $G_{\upsilon''}^0$ refer to the upper and lower states, respectively.

The term values of the lower state levels were calculated using the parameters listed in Table II (see below). These were derived from the analysis of the IR data reported in Table 1 of Ref. 7, fitting simultaneously the transitions involving bending states with υ_{tot} up to 2 and the $2\nu_4 + \nu_5(^{\Pi}\Pi) \leftarrow 2\nu_4(\Delta)$ band with centre at 527.86 cm^{-1}. The addition of the last band in the data set provided the missing information on the "f" levels of the $2\nu_4(\Delta)$ state up to $J'' = 36$, which was necessary to fit together the transitions of the $\nu_3 + 2\nu_4(\Delta) \leftarrow 2\nu_4(\Delta)$ (at 2420.69 cm^{-1}) and of the $\nu_3 + 2\nu_4(\Delta) \leftarrow \nu_4(\Pi)$ (at 2928.44 cm^{-1}) bands. The former band was perfectly fitted with the parameters in Table 2 of Ref. 7, whereas in the second one, all transitions with $J' \geq 14$ reaching the "f" levels were discarded according to the rejection criterion adopted in the fit (see below). In fact, the refined parameters are suitable for the term values of the $\nu_3 + 2\nu_4(\Delta_f)$ levels aside from the $2\nu_4(\Delta_f)$ lower state term values, but they result inadequate to reproduce the transitions of the $\nu_3 + 2\nu_4(\Delta) \leftarrow \nu_4(\Pi)$ band. The parameters in Table 3 of Ref. 7 from the analysis of the transitions with υ_{tot} up to 3 were not used to calculate LSCD since all the hot bands analysed in our spectra are from levels with $\upsilon_{tot} \leq 2$. Moreover, since no transition to the $\upsilon_4 = 3$ state was identified, some parameters resulted effective.

The effects of vibrational and rovibrational perturbations were evident in the pattern of the assigned lines for a number of bands. As a consequence, it was necessary to include in Eq. (1) terms of higher order in the rotational angular momentum to achieve an adequate reproduction of the measured transition wavenumbers.

V. ANALYSIS

Once the assignment procedure was completed, all the transition wavenumbers relative to a specific stretching mode, i.e., the fundamental band, its overtone, and the hot and combination bands involving bending modes, were fitted together. In this way, three sets of spectroscopic parameters, one for each stretching mode, were obtained from independent fits.

The data were fitted to the following expressions where the vibrational and rotational diagonal contributions are $G^0(v,l)$ and $F(v,l,J)$, respectively:

TABLE I. Vibrational assignments and band centres, ν_C (in cm^{-1}), of the vibration-rotation bands for $^{13}C^{12}CD_2$.

Transition	Symmetry	ν_c[a]	P, R, Q (J_{min}, J_{max})	$\sigma(\times10^5)$[b]	Number fitted/ assigned lines
(*a*) 1900–3000 cm^{-1}					
$\nu_3+\nu_4 \leftarrow 2\nu_4$	$\Pi \leftarrow \Sigma^+$	1 918.1654	$R_{e\text{-}e}$ (0-10); $Q_{f\text{-}e}$ (1-23)	39	27/34
	$\Pi \leftarrow \Delta$	1 918.6625	$P_{e\text{-}e}$ (2-27); $R_{e\text{-}e}$ (3-24); $Q_{e\text{-}f}$ (2-21) $P_{f\text{-}f}$ (3-23); $R_{f\text{-}f}$ (2-20)	49	85/108
$\nu_3 \leftarrow \nu_4$	$\Sigma^+ \leftarrow \Pi$	1 927.1077	$P_{e\text{-}e}$ (1-35); $R_{e\text{-}e}$ (1-34); $Q_{e\text{-}f}$ (1-35)	34	104/104
$\nu_3+\nu_5 \leftarrow \nu_4+\nu_5$	$\Pi \leftarrow \Sigma^+$	1 928.5007	$P_{e\text{-}e}$ (3-23); $R_{e\text{-}e}$ (2-22); $Q_{f\text{-}e}$ (1-21)	39	51/63
$\nu_1+\nu_4 \leftarrow \nu_4+\nu_5$	$\Pi \leftarrow \Sigma^+$	2 134.6406	$P_{e\text{-}e}$ (5-21); $R_{e\text{-}e}$ (4-18); $Q_{f\text{-}e}$ (1-16)	45	37/48
$\nu_1+\nu_5 \leftarrow 2\nu_5$	$\Pi \leftarrow \Sigma^+$	2 139.4447	$P_{e\text{-}e}$ (3-25); $R_{e\text{-}e}$ (2-25); $Q_{f\text{-}e}$ (1-20)	39	59/67
	$\Pi \leftarrow \Delta$	2 134.8541	$P_{e\text{-}e}$ (2-20); $R_{e\text{-}e}$ (5-14); $Q_{e\text{-}f}$ (2-24) $P_{f\text{-}f}$ (2-22); $R_{f\text{-}f}$ (3-20); $Q_{f\text{-}e}$ (3-24)	39	92/113
$\nu_1 \leftarrow \nu_5$	$\Sigma^+ \leftarrow \Pi$	2 142.6370	$P_{e\text{-}e}$ (1-34); $R_{e\text{-}e}$ (1-31); $Q_{e\text{-}f}$ (1-33)	33	95/98
$\nu_3+2\nu_4 \leftarrow 2\nu_4$	$\Sigma^+ \leftarrow \Sigma^+$	2 420.4954	$P_{e\text{-}e}$ (1-38); $R_{e\text{-}e}$ (0-35)	24	67/74
	$\Delta \leftarrow \Delta$	2 420.6882	$P_{e\text{-}e}$ (3-42); $R_{e\text{-}e}$ (2-42) $P_{f\text{-}f}$ (3-43); $R_{f\text{-}f}$ (2-43)	38	134/164
$\nu_3+\nu_4+\nu_5 \leftarrow \nu_4+\nu_5$	$\Sigma^+ \leftarrow \Sigma^+$	2 421.2629	$P_{e\text{-}e}$ (1-41); $R_{e\text{-}e}$ (0-42)	32	74/83
	$\Sigma^- \leftarrow \Sigma^-$	2 421.6612	$P_{f\text{-}f}$ (1-46); $R_{f\text{-}f}$ (0-41)	42	65/88
	$\Delta \leftarrow \Delta$	2 421.0714	$P_{e\text{-}e}$ (3-43); $R_{e\text{-}e}$ (2-44); $Q_{e\text{-}f}$ (2-20) $P_{f\text{-}f}$ (3-43); $R_{f\text{-}f}$ (2-43); $Q_{f\text{-}e}$ (2-21)	41	152/202
$\nu_3+2\nu_5 \leftarrow 2\nu_5$	$\Sigma^+ \leftarrow \Sigma^+$	2 422.0331	$P_{e\text{-}e}$ (1-40); $R_{e\text{-}e}$ (0-38)	37	66/79
	$\Delta \leftarrow \Delta$	2 421.9636	$P_{e\text{-}e}$ (3-39); $R_{e\text{-}e}$ (2-38); $Q_{e\text{-}f}$ (2-17) $P_{f\text{-}f}$ (3-40); $R_{f\text{-}f}$ (2-40); $Q_{f\text{-}e}$ (2-13)	34	143/178
$\nu_3+\nu_4 \leftarrow \nu_4$	$\Pi \leftarrow \Pi$	2 426.4164	$P_{e\text{-}e}$ (2-52); $R_{e\text{-}e}$ (1-53); $Q_{e\text{-}f}$ (1-22) $P_{f\text{-}f}$ (2-50); $R_{f\text{-}f}$ (1-49); $Q_{f\text{-}e}$ (1-15)	28	225/239
$\nu_3+\nu_5 \leftarrow \nu_5$	$\Pi \leftarrow \Pi$	2 427.0457	$P_{e\text{-}e}$ (2-49); $R_{e\text{-}e}$ (1-52); $Q_{e\text{-}f}$ (1-22) $P_{f\text{-}f}$ (2-51); $R_{f\text{-}f}$ (1-51); $Q_{f\text{-}e}$ (3-22)	27	231/241
$\nu_3 \leftarrow$ GS	$\Sigma^+ \leftarrow \Sigma^+$	2 432.0810	$P_{e\text{-}e}$ (1-52); $R_{e\text{-}e}$ (0-53)	32	103/106
$\nu_1+\nu_4 \leftarrow \nu_5$	$\Pi \leftarrow \Pi$	2 633.1857	$P_{e\text{-}e}$ (2-26); $R_{e\text{-}e}$ (1-28) $P_{f\text{-}f}$ (2-26); $R_{f\text{-}f}$ (1-29)	32	94/107
$\nu_1+\nu_4+\nu_5 \leftarrow \nu_4+\nu_5$	$\Sigma^+ \leftarrow \Sigma^+$	2 656.8181	$P_{e\text{-}e}$ (1-24); $R_{e\text{-}e}$ (0-23)	31	40/48
	$\Sigma^- \leftarrow \Sigma^-$	2 656.3712	$P_{f\text{-}f}$ (1-23); $R_{f\text{-}f}$ (1-25)	42	35/48
	$\Delta \leftarrow \Delta$	2 657.0344	$P_{e\text{-}e}$ (3-25); $R_{e\text{-}e}$ (2-25) $P_{f\text{-}f}$ (3-25); $R_{f\text{-}f}$ (2-22)	49	64/91
$\nu_1+2\nu_5 \leftarrow 2\nu_5$	$\Sigma^+ \leftarrow \Sigma^+$	2 662.8665	$P_{e\text{-}e}$ (1-26); $R_{e\text{-}e}$ (0-26)	39	42/53
	$\Delta \leftarrow \Delta$	2 662.9268	$P_{e\text{-}e}$ (3-22); $R_{e\text{-}e}$ (2-21) $P_{f\text{-}f}$ (3-23); $R_{f\text{-}f}$ (2-23)	36	59/83
$\nu_1+\nu_4 \leftarrow \nu_4$	$\Pi \leftarrow \Pi$	2 664.8463	$P_{e\text{-}e}$ (2-36); $R_{e\text{-}e}$ (1-35); $Q_{e\text{-}f}$ (1-9) $P_{f\text{-}f}$ (2-32); $R_{f\text{-}f}$ (1-32); $Q_{f\text{-}e}$ (1-10)	24	136/152
$\nu_1+\nu_5 \leftarrow \nu_5$	$\Pi \leftarrow \Pi$	2 671.0971	$P_{e\text{-}e}$ (2-36); $R_{e\text{-}e}$ (1-37) $P_{f\text{-}f}$ (2-36); $R_{f\text{-}f}$ (1-36)	27	130/143
$\nu_1 \leftarrow$ GS[c]	$\Sigma^+ \leftarrow \Sigma^+$	2 679.2709	$Q_{e\text{-}e}$ (0-34)	55	35/35
$\nu_1 \leftarrow$ GS	$\Sigma^+ \leftarrow \Sigma^+$	2 679.2709	$P_{e\text{-}e}$ (1-43); $R_{e\text{-}e}$ (0-47)	28	87/91
$\nu_1+\nu_5 \leftarrow \nu_4$	$\Pi \leftarrow \Pi$	2 702.7577	$P_{e\text{-}e}$ (2-30); $R_{e\text{-}e}$ (1-28) $P_{f\text{-}f}$ (2-30); $R_{f\text{-}f}$ (1-28)	36	103/114
$\nu_3+\nu_4+\nu_5 \leftarrow \nu_5$	$\Sigma^+ \leftarrow \Pi$	2 919.8080	$P_{e\text{-}e}$ (1-35); $R_{e\text{-}e}$ (1-25); $Q_{e\text{-}f}$ (1-26)	44	72/86
	$\Sigma^- \leftarrow \Pi$	2 926.8159	$P_{f\text{-}f}$ (1-30); $R_{f\text{-}f}$ (1-21); $Q_{f\text{-}e}$ (5-31)	51	62/77
	$\Delta \leftarrow \Pi$	2 926.0061	$P_{e\text{-}e}$ (3-27); $R_{e\text{-}e}$ (1-27); $Q_{e\text{-}f}$ (2-36) $P_{f\text{-}f}$ (4-31); $R_{f\text{-}f}$ (1-25); $Q_{f\text{-}e}$ (2-26)	46	114/164
$\nu_3+2\nu_4 \leftarrow \nu_4$	$\Sigma^+ \leftarrow \Pi$	2 928.7463	$P_{e\text{-}e}$ (2-16); $Q_{e\text{-}f}$ (1-28)	41	38/43
	$\Delta \leftarrow \Pi$	2 928.4421	$P_{e\text{-}e}$ (3-38); $R_{e\text{-}e}$ (1-29); $Q_{e\text{-}f}$ (8-12) $P_{f\text{-}f}$ (3-30); $R_{f\text{-}f}$ (1-29)	37	107/127
$\nu_3+\nu_4 \leftarrow$ GS	$\Pi \leftarrow \Sigma^+$	2 931.3896	$P_{e\text{-}e}$ (2-46); $R_{e\text{-}e}$ (0-34); $Q_{f\text{-}e}$ (4-41)	32	112/118
(*b*) 3000–5000 cm^{-1}					
$\nu_1+\nu_4+\nu_5 \leftarrow \nu_4$	$\Sigma^+ \leftarrow \Pi$	3 187.0237	$P_{e\text{-}e}$ (1-27); $R_{e\text{-}e}$ (1-29); $Q_{e\text{-}f}$ (1-27)	38	60/83
	$\Sigma^- \leftarrow \Pi$	3 193.1865	$P_{f\text{-}f}$ (1-27); $R_{f\text{-}f}$ (1-28); $Q_{f\text{-}e}$ (1-30)	34	48/85
	$\Delta \leftarrow \Pi$	3 193.6297	$P_{e\text{-}e}$ (3-26); $R_{e\text{-}e}$ (1-24); $Q_{e\text{-}f}$ (2-31) $P_{f\text{-}f}$ (6-27); $R_{f\text{-}f}$ (1-25); $Q_{f\text{-}e}$ (2-18)	43	94/141
$\nu_1+2\nu_5 \leftarrow \nu_5$	$\Sigma^+ \leftarrow \Pi$	3 194.5189	$P_{e\text{-}e}$ (1-33); $R_{e\text{-}e}$ (1-33); $Q_{e\text{-}f}$ (1-27)	40	70/93
	$\Delta \leftarrow \Pi$	3 199.1698	$P_{e\text{-}e}$ (5-27); $R_{e\text{-}e}$ (1-27); $Q_{e\text{-}f}$ (2-30) $P_{f\text{-}f}$ (3-27); $R_{f\text{-}f}$ (1-29); $Q_{f\text{-}e}$ (2-28)	30	129/159
$\nu_1+\nu_5 \leftarrow$ GS	$\Pi \leftarrow \Sigma^+$	3 207.7310	$P_{e\text{-}e}$ (2-38); $R_{e\text{-}e}$ (0-40); $Q_{f\text{-}e}$ (1-39)	27	109/115
$\nu_3+2\nu_4 \leftarrow$ GS	$\Sigma^+ \leftarrow \Sigma^+$	3 433.7196	$P_{e\text{-}e}$ (1-26); $R_{e\text{-}e}$ (0-28)	40	52/55
$\nu_3+2\nu_4 \leftarrow$ GS[d]	$(\Delta \leftarrow \Sigma^+)$	3 433.4153	$P_{e\text{-}e}$ (6-29); $R_{e\text{-}e}$ (3-31)	49	45/53
$\nu_3+\nu_4+\nu_5 \leftarrow$ GS	$\Sigma^+ \leftarrow \Sigma^+$	3 456.4419	$P_{e\text{-}e}$ (2-23); $R_{e\text{-}e}$ (1-22)	41	40/44
$\nu_3+2\nu_5 \leftarrow$ GS	$\Sigma^+ \leftarrow \Sigma^+$	3 490.3194	$P_{e\text{-}e}$ (1-28); $R_{e\text{-}e}$ (0-32)	39	60/61
$\nu_1+\nu_4+\nu_5 \leftarrow$ GS	$\Sigma^+ \leftarrow \Sigma^+$	3 691.9970	$P_{e\text{-}e}$ (1-37); $R_{e\text{-}e}$ (0-35)	21	66/73
$\nu_2+\nu_3+\nu_4 \leftarrow \nu_4$	$\Pi \leftarrow \Pi$	4 157.6846	$P_{e\text{-}e}$ (2-35); $R_{e\text{-}e}$ (1-31) $P_{f\text{-}f}$ (2-34); $R_{f\text{-}f}$ (1-31)	31	119/129

TABLE I. (*Continued.*)

Transition	Symmetry	ν_c[a]	P, R, Q (J_{min}, J_{max})	$\sigma(\times10^5)$[b]	Number fitted/ assigned lines
$\nu_2+\nu_3+\nu_5 \leftarrow \nu_5$	$\Pi \leftarrow \Pi$	4 163.8527	$P_{e\text{-}e}$ (2-30); $R_{e\text{-}e}$ (1-24) $P_{f\text{-}f}$ (3-30); $R_{f\text{-}f}$ (1-31)	32	102/112
$\nu_2+\nu_3 \leftarrow$ GS	$\Sigma^+ \leftarrow \Sigma^+$	4 167.4672	$P_{e\text{-}e}$ (1-42); $R_{e\text{-}e}$ (0-39)	27	80/82
$2\nu_3 \leftarrow$ GS	$\Sigma^+ \leftarrow \Sigma^+$	4 834.4642	$P_{e\text{-}e}$ (1-34); $R_{e\text{-}e}$ (0-36)	39	65/71
(c) 5000–8000 cm^{-1}					
$\nu_1+\nu_3+\nu_4 \leftarrow \nu_4$	$\Pi \leftarrow \Pi$	5 044.0960	$P_{e\text{-}e}$ (2-40); $R_{e\text{-}e}$ (1-38) $P_{f\text{-}f}$ (2-40); $R_{f\text{-}f}$ (1-38)	28	131/154
$\nu_1+\nu_3+\nu_5 \leftarrow \nu_5$	$\Pi \leftarrow \Pi$	5 050.8745	$P_{e\text{-}e}$ (2-41); $R_{e\text{-}e}$ (1-38) $P_{f\text{-}f}$ (2-41); $R_{f\text{-}f}$ (1-38)	31	138/156
$\nu_1+\nu_3 \leftarrow$ GS	$\Sigma^+ \leftarrow \Sigma^+$	5 064.1724	$P_{e\text{-}e}$ (1-48); $R_{e\text{-}e}$ (0-47)	36	84/96
$\nu_2+\nu_3+2\nu_4 \leftarrow$ GS	$\Sigma^+ \leftarrow \Sigma^+$	5 162.0874	$P_{e\text{-}e}$ (1-29); $R_{e\text{-}e}$ (0-27)	46	54/57
$2\nu_1 \leftarrow$ GS	$\Sigma^+ \leftarrow \Sigma^+$	5 334.2740	$P_{e\text{-}e}$ (1-29); $R_{e\text{-}e}$ (0-27)	41	45/57
$2\nu_3+\nu_5 \leftarrow$ GS	$\Pi \leftarrow \Sigma^+$	5 361.0017	$P_{e\text{-}e}$ (2-32); $R_{e\text{-}e}$ (0-25); $Q_{f\text{-}e}$ (1-31)	42	81/88
$\nu_1+\nu_2+\nu_4+\nu_5 \leftarrow$ GS	$\Sigma^+ \leftarrow \Sigma^+$	5 418.4221	$P_{e\text{-}e}$ (2-21); $R_{e\text{-}e}$ (1-22)	43	39/42
$2\nu_1+\nu_5 \leftarrow$ GS	$\Pi \leftarrow \Sigma^+$	5 854.7281	$P_{e\text{-}e}$ (2-30); $R_{e\text{-}e}$ (0-28); $Q_{f\text{-}e}$ (1-35)	44	78/93
$2\nu_1+\nu_4+\nu_5 \leftarrow$ GS[e]	$\Sigma^+ \leftarrow \Sigma^+$	6 324.4484	$P_{e\text{-}e}$ (1-24); $R_{e\text{-}e}$ (0-30)	112	44/55
$\nu_1+\nu_2+\nu_3+\nu_4 \leftarrow \nu_4$[e]	$\Pi \leftarrow \Pi$	6 755.5980	$P_{e\text{-}e}$ (2-34); $R_{e\text{-}e}$ (1-28) $P_{f\text{-}f}$ (2-34); $R_{f\text{-}f}$ (1-28)	117	86/122
$\nu_1+\nu_2+\nu_3+\nu_5 \leftarrow \nu_5$[e]	$\Pi \leftarrow \Pi$	6 768.1405	$P_{e\text{-}e}$ (2-35); $R_{e\text{-}e}$ (1-25) $P_{f\text{-}f}$ (2-37); $R_{f\text{-}f}$ (1-25)	109	91/120
$\nu_1+\nu_2+\nu_3 \leftarrow$ GS[e]	$\Sigma^+ \leftarrow \Sigma^+$	6 780.0709	$P_{e\text{-}e}$ (1-44); $R_{e\text{-}e}$ (0-34)	41	76/78
$3\nu_3 \leftarrow$ GS	$\Sigma^+ \leftarrow \Sigma^+$	7 207.1658	$P_{e\text{-}e}$ (1-28); $R_{e\text{-}e}$ (0-24)	104	47/53
$2\nu_1+\nu_3 \leftarrow$ GS	$\Sigma^+ \leftarrow \Sigma^+$	7 674.9864	$P_{e\text{-}e}$ (1-29); $R_{e\text{-}e}$ (0-30)	51	54/60
$2\nu_1+2\nu_2+\nu_3 \leftarrow$ GS[f]	$\Sigma^+ \leftarrow \Sigma^+$	11 058.867	$P_{e\text{-}e}$ (-15); $R_{e\text{-}e}$ (-17)	490	20/27
$\nu_1+\nu_2+3\nu_3 \leftarrow$ GS[f]	$\Sigma^+ \leftarrow \Sigma^+$	11 431.848	$P_{e\text{-}e}$ (-31); $R_{e\text{-}e}$ (-36)	550	45/59

[a]The band centre, ν_C, is defined as $\nu_C = G^0_{v'} - B_{v'}k^2 - D_{v'}k^4 - (G^0_{v''} - B_{v''}k^2 - D_{v''}k^4)$ (see text).

[b]σ (in cm^{-1}) corresponds to the RMS value of the residuals for the various fitted lines resulting from the simultaneous fit (see text).

[c]Raman band.

[d]Perturbation allowed transition.

[e]From Ref. 11.

[f]From Ref. 10.

$$G^0(v,l) = \sum_{i=1,5} \omega_i^0 v_i + \sum_{i\le j} x_{ij}^0 v_i v_j + \sum_{b\le b'=4,5} g_{l_b l_{b'}} l_b l_{b'} + \sum_{i\le j\le m} y_{ijm} v_i v_j v_m + \sum_{i,b\le b'} y_i^{l_b l_{b'}} v_i l_b l_{b'} + \sum_{i\le j\le m\le n} y_{ijmn} v_i v_j v_m v_n + \sum_{i\le j,b\le b'} y_{ij}^{l_b l_{b'}} v_i v_j l_b l_{b'}, \quad (3)$$

$$F(v,l,J) = \left[B_0 - \sum_i \alpha_i v_i + \sum_{i\le j} \gamma_{ij} v_i v_j + \sum_{b\le b'=4,5} \gamma^{l_b l_{b'}} l_b l_{b'} + \sum_{i\le j\le m} \gamma_{ijm} v_i v_j v_m + \sum_{i,b\le b'=4,5} \gamma_i^{l_b l_{b'}} v_i l_b l_{b'}\right][M-k^2] - \left[D_0 + \sum_i \beta_i v_i + \sum_{i\le j} \delta_{ij} v_i v_j + \sum_{b\le b'} \delta^{l_b l_{b'}} l_b l_{b'} + \sum_{i\le j\le m} \delta_{ijm} v_i v_j v_m + \sum_{i,b\le b'=4,5} \delta_i^{l_b l_{b'}} v_i l_b l_{b'}\right][M-k^2]^2 + \left[H_0 + \sum_i h_i v_i\right][M-k^2]^3. \quad (4)$$

Vibrational and rotational l-type resonance contributions for the bending levels are expressed by off-diagonal matrix elements, see Table I of Ref. 23, containing the following parameters:

$$r_{45} = r_{45}^0 + r_{45t} v_t + r_{45}^J M + r_{45}^{JJ} M^2 + r_{45}^{JJJ} M^3, \quad (5)$$

$$q_t = q_t^0 + q_{tt} v_t + q_{tt'} v_{t'} + q_t^J M + q_t^{JJ} M^2 + q_t^k (k\pm1)^2, \quad (6)$$

$$\rho_t = \rho_t^0 + \rho_{tt} v_t + \rho_{tt'} v_{t'} + \rho_t^J M + \rho_t^{JJ} M^2, \quad (7)$$

and

$$\rho_{45}^0 + \rho_{45}^J M + \rho_{45}^{JJ} M^2. \quad (8)$$

Moreover, the r, q, and ρ parameters for the energy levels involving simultaneously one stretching v_s (s = 1, 2, 3) and bending modes are given by the expressions

$$r_{s45} = r_{s45}^0 + r_{s45}^J M + r_{s45}^{JJ} M^2, \quad (9)$$

$$q_{st} = q_{st}^0 + q_{stt} v_t + q_{stt'} v_{t'} + q_{ss't} v_{s'} v_t + q_{st}^J M + q_{st}^{JJ} M^2, \quad (10)$$

$$\rho_{st} = \rho_{st}^0 + \rho_{st}^J M + \rho_{st}^{JJ} M^2 + \rho_{st}^{JJJ} M^3, \quad (11)$$

$$\rho_{s45} = \rho_{s45}^0 + \rho_{s45}^J M, \quad (12)$$

with $M = J(J+1)$ and $t, t' = 4$ or 5.

Finally, because the separation between ν_4 and ν_5 bending modes is merely 32 cm^{-1}, vibrational coupling of D–D

TABLE II. Spectroscopic parameters (in cm^{-1}) for the bending modes of $^{13}C^{12}CD_2$ resulting from the simultaneous fit of all levels with $\nu_4+\nu_5 \le 2$ and the band $2\nu_4+\nu_5(^{II}\Pi) \leftarrow 2\nu_4(\Delta)$.[a]

Parameter/(cm^{-1})	
ω_4^0	503.558 854 7(924)
ω_5^0	536.845 712 1(573)
x_{44}^0	1.725 718(521)
x_{45}^0	−1.577 150 8(495)
x_{55}^0	−1.550 370(518)
g_{44}^0	0.523 717(518)
g_{45}^0	3.216 433 8(304)
g_{55}^0	2.173 704(519)
r_{45}^0	−3.304 829 3(420)
$r_{45}^J \times 10^3$	0.086 819(133)
B_0	0.833 118 683(474)
$\alpha_4 \times 10^3$	−1.946 066(209)
$\alpha_5 \times 10^3$	−2.075 198(103)
$\gamma_{44} \times 10^3$	−0.012 770 9(741)
$\gamma_{45} \times 10^3$	0.001 540(132)
$\gamma_{55} \times 10^3$	0.009 246 2(376)
$\gamma^{44} \times 10^3$	−0.015 198(107)
$\gamma^{45} \times 10^3$	−0.079 024(108)
$\gamma^{55} \times 10^3$	−0.039 955 9(673)
$D_0 \times 10^6$	0.772 430(194)
$\beta_4 \times 10^6$	0.020 715 8(769)
$\beta_5 \times 10^6$	0.017 019 2(359)
$\delta_{45} \times 10^9$	−1.285 6(711)
$\delta^{45} \times 10^9$	−1.305(100)
$q_4^0 \times 10^3$	3.167 028(111)
$q_5^0 \times 10^3$	3.167 525 0(867)
$q_{45} \times 10^3$	0.020 905(340)
$q_4^J \times 10^6$	−0.021 117 8(852)
$q_5^J \times 10^6$	−0.020 675 4(514)
$q_5^k \times 10^3$	0.031 405(117)
$\rho_5^0 \times 10^6$	−0.002 704(106)
$\rho_{45}^0 \times 10^6$	0.004 748(330)
$K_{44,55}^0$	−6.573 89(843)
Number of fitted/assigned data	1632/1782
Standard deviation of the fit (cm^{-1})	0.000 365

[a]Estimated uncertainties (1σ) are given in parentheses in units of the last figure quoted.

type occurs between levels of identical symmetry, such as $\upsilon_4 = 2$ (Σ^+ and Δ) and $\upsilon_5 = 2$ (Σ^+ and Δ), associated with each stretching mode. This interaction, which has been treated in detail for the pure bending states,[7] has been taken into account in the global fitting procedures of both the pure bending levels and of the stretching-bending ones. The off-diagonal matrix elements (see Table I of Ref. 23, where $s_{s45} \equiv K_{s44,s55}$) contain the parameters in the following equation:

$$K_{s44,s55} = K^0_{s44,s55} + K^J_{s44,s55}M + K^{JJ}_{s44,s55}M^2, \qquad (13)$$

where the subscript $s = 1, 2, 3$ refers to one of the stretching modes, for Σ^+ interacting states. For interacting Δ states, the parameters are g_{45}, r_{45}, or r_{s45}, as defined in Eqs. (3), (5), and (9). The complete block-diagonalized matrices illustrating the l-type and the D–D interactions between the bending levels in the various vibrational manifolds are reported in Table II of Ref. 23.

The stretching-stretching combination bands involving $\nu_1 + \nu_2$ (Σ^+), $\nu_1 + \nu_3$ (Σ^+) and $\nu_2 + \nu_3$ (Σ^+), with associated hot and combination bands, were fitted separately. All the vibration and rotation parameters related to the $\upsilon_s = 1$ ($s = 1, 2, 3$) states in Eqs. (3) and (4), i.e., $\omega_s^0, x_{ss}^0, \alpha_s, \beta_s$, etc., were constrained to the values obtained from the analysis of the corresponding stretching band system.

In the simultaneous fits, the ground state and the pure bending state parameters were held fixed to the values reported in Table II. Identical unitary weights were assigned to all transitions with the exclusion of the overlapping lines, which were given zero weight. Finally, transition wavenumbers that differed from the corresponding calculated values by more than 0.001 cm^{-1} (~2.5 times their estimated uncertainties) were excluded from the last cycle of the least-squares procedure.

The structure of the dataset conditioned the choice of the refined parameters in each simultaneous fit. An identical strategy was adopted: first, the bands with $\upsilon_s = 1$, 2, and 3 ($s = 1$, 2, 3) as upper states were fitted. The transitions to the corresponding associated bending states were successively added in blocks, starting with those involving $\upsilon_4 = 1$ and $\upsilon_5 = 1$, then including the manifold $\upsilon_4 = \upsilon_5 = 1$ ($\Sigma^+, \Sigma^-, \Delta$) and, finally, the $\upsilon_4 = 2$ and $\upsilon_5 = 2$, Σ^+ and Δ states, coupled by the D–D interaction. The enlargement of the dataset required the refinement of the appropriate higher order parameters, which were chosen according to the following constraints: they must correspond to lower-order constants previously refined, be statistically determined, and improve the quality of the fit. After each fit, the statistical significance of the obtained parameters was checked as well as their correlation coefficients. The results of the simultaneous analysis were compared to those achieved in the single band fits to support the adequacy of the adopted Hamiltonian model.

VI. RESULTS AND DISCUSSION

The RMS values of the residuals for the fitted lines in the σ column of Table I attest to the good quality of the fit. With the exception of the value for the $3\nu_3 \leftarrow$ GS band, these are all better than 0.0005 cm^{-1}. Precise values for the band centres, whose uncertainties are usually of the order of a few units in 10^{-4} cm^{-1}, are also reported in Table I.

Most of the parameters for the bending states listed in Table II are in good agreement with the corresponding ones in Table 2 of Ref. 7. As expected, the value of the γ^{44} constant, which is responsible for the "*e*," "*f*" splittings of the $2\nu_4$ (Δ) levels, exhibits the largest difference (~31%). Differences between 1% and 6% are also observed for the parameters related to the υ_4 and υ_5 modes, γ_{45}, q_{45}, q_4^J, ρ_5^0, ρ_{45}^0, q_5^k, δ_{45}, δ^{45}, and $K_{44,55}^0$.

The parameters obtained for each stretching or stretching–stretching system, together with the number of transitions assigned and retained in the final fit, according to the above mentioned criterion for rejection, are listed in Tables III–VII. To favour the comparison between corresponding parameters, they are reported in the same units in all the tables.

The parameters of the model present in Eqs. (3), (4), (9)–(12), which are not reported in Tables III–VII, were

TABLE III. Spectroscopic parameters (in cm^{-1}) of $^{13}C^{12}CD_2$ resulting from the simultaneous fit of ν_1 and associated hot bands.[a]

Parameter/(cm^{-1})	
ω_1^0	2691.404 800 8(912)
x_{11}^0	−12.133 887 0(618)
x_{14}^0	−14.430 158 4(534)
x_{15}^0	−8.255 400(114)
y_{145}	−0.109 769(185)
y_{155}	−0.005 177 1(291)
y_{115}	0.083 962 1(667)
y_1^{45}	0.208 782 8 (327)
y_1^{55}	−0.002 853 3(157)
r_{145}^0	−3.081 389 0(385)
$r_{145}^J \times 10^3$	0.082 757(136)
$\alpha_1 \times 10^3$	5.722 665(324)
$\gamma_{11} \times 10^3$	0.070 533(265)
$\gamma_{14} \times 10^3$	0.110 002(211)
$\gamma_{15} \times 10^3$	0.005 976(199)
$\gamma_{145} \times 10^3$	0.036 464(499)
$\gamma_{115} \times 10^3$	−0.012 728(168)
$\gamma_1^{45} \times 10^3$	−0.004 545(148)
$\beta_1 \times 10^6$	−0.001 986(322)
$\delta_{11} \times 10^9$	2.557(305)
$\delta_{14} \times 10^9$	1.876(190)
$q_{14}^0 \times 10^3$	3.218 881(287)
$q_{15}^0 \times 10^3$	3.113 931(474)
$q_{145}^0 \times 10^3$	0.079 727(548)
$q_{155} \times 10^3$	0.034 147(176)
$q_{115} \times 10^3$	0.073 259(342)
$q_{14}^J \times 10^6$	−0.026 726(351)
$q_{15}^J \times 10^6$	−0.022 293(151)
$K_{144,155}^0$	−7.1[b]
$K_{144,155}^J \times 10^3$	−0.030 53(111)
Number of fitted/assigned data	1807/2190
Standard deviation of the fit (cm^{-1})	0.000 357

[a]Estimated uncertainties (1σ) are given in parentheses in units of the last figure quoted.
[b]Constrained (see text).

TABLE IV. Spectroscopic parameters (in cm^{-1}) of $^{13}C^{12}CD_2$ resulting from the simultaneous fit of ν_2 and associated hot bands.[a]

Parameter/(cm^{-1})	
ω_2^0	1752.174 769(117)
x_{22}^0	−4.382 578 2(738)
x_{24}^0	−4.371 581(161)
x_{25}^0	1.517 795(157)
y_{244}	0.316 697 4(920)
y_{245}	−0.078 117(112)
y_2^{44}	−0.234 287 8(892)
y_2^{55}	−0.039 914 4(767)
y_2^{45}	−0.027 828 7(321)
r_{245}^0	−3.276 226 3(533)
$r_{245}^J \times 10^3$	0.084 606(246)
$\alpha_2 \times 10^3$	3.109 181(366)
$\gamma_{22} \times 10^3$	−0.002 257(234)
$\gamma_{24} \times 10^3$	−0.072 391(786)
$\gamma_{25} \times 10^3$	−0.063 181(616)
$\gamma_{245} \times 10^3$	0.006 161(554)
$\gamma_2^{44} \times 10^3$	0.005 694(554)
$\gamma_2^{55} \times 10^3$	0.003 718(379)
$\beta_2 \times 10^6$	0.000 480(133)
$\delta_{24} \times 10^9$	−27.64(139)
$\delta_{25} \times 10^9$	−42.20(136)
$\delta_{245} \times 10^9$	11.083(738)
$\delta_2^{44} \times 10^9$	22.18(121)
$\delta_2^{55} \times 10^9$	39.99(128)
$q_{24}^0 \times 10^3$	3.223 90(122)
$q_{25}^0 \times 10^3$	3.159 11(306)
$q_{244}^0 \times 10^3$	−0.035 52(106)
$q_{245}^0 \times 10^3$	0.058 289(951)
$q_{255}^0 \times 10^3$	0.110 73(298)
$q_{24}^J \times 10^6$	−0.020 616(554)
$q_{25}^J \times 10^6$	−0.018 905(339)
$\rho_{24}^0 \times 10^6$	−0.059 43(344)
$\rho_{25}^0 \times 10^6$	−0.134 58(423)
$K_{244,255}^0$	−5.902 33(156)
$K_{244,255}^J \times 10^3$	−0.178 91(724)
Number of fitted/assigned data	1085/1236
Standard deviation of the fit (cm^{-1})	0.000 455

[a]Estimated uncertainties (1σ) are given in parentheses in units of the last figure quoted.

nevertheless refined in the fitting procedure, but they resulted statistically undetermined and were constrained to zero.

In total, 5314 out of 6229 transitions assigned to ν_1, ν_2, and ν_3 stretching–bending system were retained in the final fits, 915 of them (about 15%) were discarded because they were overlapping (689) or their observed—calculated values exceed the chosen tolerance (226). Twenty nine parameters for ν_1, 35 for ν_2, and 36 for ν_3 were determined with high precision. They include, in addition to the l-type constants, the D–D interaction coefficients. The $K_{144,155}^0$ constant was fixed to −0.71 cm^{-1}, obtained scaling the $K_{344,355}^0$ value in Table V according to the ratio between $K_{344,355}^0$ and $K_{144,155}^0$ in $^{12}C_2D_2$.[19] In fact, $K_{144,155}^0$ could not be refined owing to the lack of information on the $\nu_1 + 2\nu_4$ levels interacting with those of $\nu_1 + 2\nu_5$, which were observed both from ν_5 and $2\nu_5$ (see Table I). The standard deviation of each fit is smaller than 0.0005 cm^{-1} of the same order of magnitude of the estimated uncertainty of the experimental measurements.

The transitions relative to the C≡C stretching (ν_2) and associated bendings listed in Table 1 of Ref. 8 have been newly fitted, using the parameters in Table II to calculate the term values of the lower levels. This was needed in order to obtain a consistent set of parameters for all the stretching modes. A comparison of the results in Table IV with those in Table 2 of Ref. 8 evidences that the quality of the fits (number of fitted transitions and standard deviation of the fit) is nearly identical. Lower correlations between the parameters were observed refining y_2^{44} and constraining y_{255} to zero. As a consequence, most of the parameters have close values in both sets but large differences are observed between some higher order constants, i.e., 50% for y_{245}, 67% for y_2^{55}, 41% for γ_{245}, and 15% for q_{244}.

A comparison between the leading constants of the rotational and vibrational l-type and D–D interactions, q_{i4}^0, q_{i5}^0, r_{i45}^0, and $K_{i44,i55}^0$, in ν_1, ν_2, and ν_3 (see Tables III–V) shows differences between 0.2% and 20%. The same parameters compare

TABLE V. Spectroscopic parameters (in cm^{-1}) of $^{13}C^{12}CD_2$ resulting from the simultaneous fit of ν_3 and associated hot bands.[a]

Parameter/(cm^{-1})	
ω_3^0	2446.935 209(166)
x_{33}^0	−14.856 946(183)
x_{34}^0	−5.625 440 7(743)
x_{35}^0	−5.006 321(124)
y_{344}	−0.043 455 8(354)
y_{345}	−0.072 794(114)
y_{355}	−0.042 551 9(401)
y_{333}	0.002 693 3(440)
y_{335}	−0.012 944 5(559)
y_3^{45}	−0.203 845 9(257)
y_3^{55}	0.022 320 3(280)
r_{345}^0	−3.503 962 1(337)
$r_{345}^J \times 10^3$	0.087 981 8(714)
$\alpha_3 \times 10^3$	4.316 416(387)
$\gamma_{33} \times 10^3$	−0.005 906(445)
$\gamma_{34} \times 10^3$	0.025 120(111)
$\gamma_{35} \times 10^3$	0.043 036 2(950)
$\gamma_{333} \times 10^3$	−0.000 853 7(991)
$\gamma_{335} \times 10^3$	0.000 505 7(557)
$\gamma_3^{44} \times 10^3$	−0.000 817 0(426)
$\gamma_3^{45} \times 10^3$	0.008 455 3(582)
$\gamma_3^{55} \times 10^3$	0.002 902 9(491)
$\beta_3 \times 10^6$	−0.005 844(152)
$\delta_{33} \times 10^9$	1.016(143)
$\delta_{34} \times 10^9$	0.251 8(391)
$\delta_{345} \times 10^9$	0.757 4(806)
$q_{34}^0 \times 10^3$	3.169 140(172)
$q_{35}^0 \times 10^3$	3.135 024(376)
$q_{344} \times 10^3$	0.002 149 5(734)
$q_{345} \times 10^3$	0.046 630(144)
$q_{355} \times 10^3$	0.032 221(103)
$q_{335} \times 10^3$	−0.070 804(237)
$q_{34}^J \times 10^6$	−0.021 462 2(586)
$q_{35}^J \times 10^6$	−0.020 659 5(702)
$K_{344,355}^0$	−7.298 293(308)
$K_{344,355}^J \times 10^3$	0.004 950(531)
Number of fitted/assigned data	2422/2803
Standard deviation of the fit (cm^{-1})	0.000 400

[a]Estimated uncertainties (1σ) are given in parentheses in units of the last figure quoted.

TABLE VI. Spectroscopic parameters (in cm^{-1}) of $^{13}C^{12}CD_2$ obtained from the fits of $\nu_1+\nu_3$, $\nu_2+\nu_3$, and associated hot bands.[a]

Parameter/(cm^{-1})[b]	$\nu_1+\nu_3$	$\nu_2+\nu_3$
x_{i3}^0	−48.670 665(147)	−12.403 251 4(574)
y_{i34}	0.012 741 2(780)	−0.167 49(127)
y_{i35}	−0.017 870 6(772)	−0.073 211 6(789)
y_{ii3}	1.493 854 5(826)	
y_{i344}		0.335 59(127)
$\gamma_{i3} \times 10^3$	−0.139 761(422)	0.078 014 4(768)
$\gamma_{i34} \times 10^3$	0.000 828 2(990)	0.007 805(321)
$\gamma_{i35} \times 10^3$	−0.000 482 5(964)	0.004 752(155)
$\gamma_{ii3} \times 10^3$	0.056 118(326)	
$\delta_{i3} \times 10^9$	−10.969(369)	
$\delta_{i34} \times 10^9$		6.248(295)
$\delta_{ii3} \times 10^9$	8.674(348)	
$q_{i34}^0 \times 10^3$	3.206 745(294)	3.197 884(409)
$q_{i35}^0 \times 10^3$	3.128 215(278)	3.138 279(509)
$q_{i34}^J \times 10^6$	−0.024 935(250)	−0.020 515(475)
$q_{i35}^J \times 10^6$	−0.022 527(232)	−0.019 186(736)
$K_{344,355}^0$		−7.940 2(105)
$K_{i344,i355}^J \times 10^3$		−0.136 85(758)
Number of fitted/assigned lines	407/466	355/380
Standard deviation of the fit (cm^{-1})	0.000 349	0.000 341

[a]Estimated uncertainties (1σ) are given in parentheses in units of the last figure quoted.
[b]i = 1 or 2, respectively.

well with the corresponding ones in the bending states (see Table II), differences being between 0.1% and 11%.

As far as the stretching-stretching combination bands are concerned, all the vibration and rotation constants of each stretching mode present in the combination states were constrained to the values listed in Tables III–V. In the case of $\nu_1 + \nu_2$, only 4 effective parameters were determined, see Table VII, because only one band, i.e., $\nu_1 + \nu_2 + \nu_4 + \nu_5$ (Σ^+) ← GS, was observed, whereas for both $\nu_1 + \nu_3$ and $\nu_2 + \nu_3$, 14 parameters were refined. No transition involving $\upsilon_{tot} = 2$ accompanying $\nu_1 + \nu_3$ was identified, whereas for $\nu_2 + \nu_3$, only the $\nu_2 + \nu_3 + 2\nu_4$ (Σ^+) ← GS band was observed, so the $K_{344,355}^0$ D–D interaction constant could be determined.

Most of the parameters are statistically very well determined; their estimated uncertainties being several orders of magnitude smaller than their values. Also, low internal correlations are generally observed between them. Only few higher order constants have uncertainties that are larger than 10% of their values. The obtained parameters can be compared with those reported for $^{12}C_2D_2$[19] and, in part, for $^{13}C_2D_2$.[20–22] The leading vibration, rotation, and interaction constants are collected in Table VIII for the three isotopologues. The values of all the common parameters agree both in sign and order of magnitude and their differences, going from $^{12}C_2D_2$ to $^{13}C_2D_2$, are in the range 0.1%–10%, with the exception of $K_{244,255}^0$, whose values differ by more than 20%.

As a consequence, the size of the D–D perturbations depends only on the energy difference between the interacting states. In $^{13}C^{12}CD_2$, it is similar for the pure bendings and for the bendings associated with the stretching modes since the values of ΔG are close, ΔG = 55.06 cm^{-1} (υ_s = 0), ΔG = 65.04 cm^{-1} (υ_2 = 1), ΔG = 56.60 cm^{-1} (υ_3 = 1), and ΔG = 67.48 cm^{-1} (υ_1 = 1), the last value being only approximately calculated, see Table IX. Owing to the closeness of the *trans* and *cis* bending states in all the fully deuterated acetylene, the D–D interaction is very efficient even at low vibrational

TABLE VII. Spectroscopic parameters (in cm^{-1}) of $^{13}C^{12}CD_2$ obtained from the fit of $\nu_1+\nu_2+\nu_4+\nu_5$.[a]

Parameter/(cm^{-1})	
x_{12}^0	−21.251 026(186)
$\gamma_{12} \times 10^3$	0.151 08(370)
$\delta_{12} \times 10^9$	1884.1(174)
$h_{12} \times 10^9$	0.458 1(220)
Number of fitted/assigned data	39/42
Standard deviation of the fit (cm^{-1})	0.000 455

[a]Estimated uncertainties (1σ) are given in parenthesis in units of the last figure quoted.

TABLE VIII. Comparison of the main vibration and rotation parameters (in cm^{-1}) of $^{12}C_2D_2$, $^{13}C^{12}CD_2$, and $^{13}C_2D_2$.[a]

Parameter/ (cm^{-1})	$^{12}C_2D_2$[b]	$^{13}C^{12}CD_2$	$^{13}C_2D_2$
ω_1^0	2717.345 212(123)	2691.404 800 8(920)	2652.469 263 7(886)[c]
ω_2^0	1769.206 582(101)	1752.174 769(117)	1729.769 308 8(689)[d]
ω_3^0	2453.899 829 6(796)	2446.935 209(166)	2426.101 140(106)[e]
x_{11}^0	−12.123 206 0(724)	−12.133 887 0(618)	0.0[f]
x_{22}^0	−4.400 340 8(641)	−4.382 578 2(738)	0.0[f]
x_{33}^0	−14.653 100 2(498)	−14.856 946(183)	0.0[f]
x_{14}^0	−15.623 572(183)	−14.430 158 4(534)	
x_{15}^0	−8.245 066 8(963)	−8.255 400(114)	
x_{24}^0	−4.014 847(153)	−4.371 581(161)	−4.711 666(209)[d]
x_{25}^0	1.706 545(140)	1.517 795(157)	1.283 986(265)[d]
x_{34}^0	−5.585 437 3(583)	−5.625 440 7(743)	−5.483 804(157)[e]
x_{35}^0	−5.152 220 0(713)	−5.006 321(124)	−5.110 157(187)[e]
r_{145}^0	−3.369 043 3(612)	−3.081 389 0(385)	
r_{245}^0	−3.545 607 8(593)	−3.276 226 3(533)	−3.465 579(139)
r_{345}^0	−3.894 696 9(355)	−3.503 962 1(337)	−3.840 404(100)[e]
$\alpha_1 \times 10^3$	5.981 994(285)	5.722 665(324)	5.383 201(706)[c]
$\alpha_2 \times 10^3$	3.162 298(170)	3.109 181(366)	3.058 969(227)[d]
$\alpha_3 \times 10^3$	4.491 143(178)	4.316 416(387)	4.161 986(164)[e]
$q_{14}^0 \times 10^3$	3.395 71(483)	3.218 881(287)	
$q_{15}^0 \times 10^3$	3.326 832(350)	3.113 930(474)	
$q_{24}^0 \times 10^3$	3.344 99(184)	3.223 90(122)	3.113 524(865)[d]
$q_{25}^0 \times 10^3$	3.240 958(935)	3.159 11(306)	2.821 01(817)[d]
$q_{34}^0 \times 10^3$	3.228 778(142)	3.169 140(172)	3.083 457(376)[e]
$q_{35}^0 \times 10^3$	3.175 816(195)	3.135 024(376)	2.977 810(462)[e]
$K_{44,55}^0$	−7.397 726 9(196)	−6.573 89(843)	−5.908 85(719)[f]
$K_{144,155}^0$	−7.678 006(650)	−7.1[g]	
$K_{244,255}^0$	−7.576 259(388)	−5.902 33(156)	−5.874 19(220)[d]
$K_{344,355}^0$	−7.898 610(231)	−7.298 293(308)	−6.619 973(807)[e]

[a]Estimated uncertainties (1σ) are given in parentheses in units of the last figure quoted.
[b]From Ref. 19.
[c]From Ref. 20.
[d]From Ref. 21.
[e]From Ref. 22.
[f]From Ref. 24.
[g]Constrained.

excitation. Moreover, the opposite sign of the x_{44}^0 and x_{55}^0 constants causes the crossing of the *trans* and *cis* bending states at relatively low energy, $n\upsilon_4 + m\upsilon_5$ with $n + m = 10$, where the effects of the perturbation are greatest. Both these characteristics account for the relevant role of these vibrations in the dynamics of the energy flow.

The parameter for the pure bending interactions, $K_{44,55}^0$, scales smoothly going from $^{12}C_2D_2$ to $^{13}C_2D_2$. The behaviour for those involving stretching excitation is more complex: a similar trend is observed for $K_{344,355}^0$, whereas it is less regular for $K_{244,255}^0$. In addition, the leading vibration and rotation parameters, ω_i^0, α_i, and the interaction constants q_{i4}^0 and q_{i5}^0 show the expected trend associated with the increased molecular masses due to the isotopic substitution.

The centre term values, G_C^0, of all the vibrationally excited states characterised in the present analysis as well as those previously studied are collected in Table IX. Thirteen term values are related to pure bending states and 51 to stretching states, including 6 values already reported in the literature.

TABLE IX. Vibrational term values, G_C^0 (in cm^{-1}), of the states involving bending and stretching modes in $^{13}C^{12}CD_2$.[a]

υ_1	υ_2	υ_3	υ_4	υ_5	ℓ_4	ℓ_5	Sym.	G_C^0
0	0	0	1	0	±1	0	Π	504.9732
0	0	0	0	1	0	±1	Π	536.6339
0	0	0	2	0	±2	0	Δ	1 012.7271
0	0	0	2	0	0	0	Σ^+	1 013.2242
0	0	0	1	1	1	−1	Σ^+	1 035.1789
0	0	0	1	1	−1	1	Σ^-	1 041.5686
0	0	0	1	1	±1	±1	Δ	1 041.7886
0	0	0	0	2	0	0	Σ^+	1 068.2863
0	0	0	0	2	0	±2	Δ	1 072.8769
0	0	0	2	1	±2	∓1	$^{II}\Pi$	1 540.5869
0	0	0	1	2	∓1	0	$^{II}\Pi$	1 566.3589[b]
0	0	0	0	3	0	±1	Π	1 599.7360[b]
0	0	0	0	3	0	±3	Π	1 608.7466[b]
0	1	0	0	0	0	0	Σ^+	1 747.7922
0	1	0	1	0	±1	0	Π	2 248.4794
0	1	0	0	1	0	±1	Π	2 285.8941
0	0	1	0	0	0	0	Σ^+	2 432.0810
1	0	0	0	0	0	0	Σ^+	2 679.2709
0	1	0	2	0	±2	0	Δ	2 752.1258
0	1	0	2	0	0	0	Σ^+	2 753.7962
0	1	0	1	1	1	−1	Σ^+	2 780.0861
0	1	0	1	1	±1	±1	Δ	2 786.4044
0	1	0	1	1	−1	1	Σ^-	2 786.6385
0	1	0	0	2	0	0	Σ^+	2 818.8318
0	1	0	0	2	0	±2	Δ	2 823.5248
0	0	1	1	0	±1	0	Π	2 931.3896
0	0	1	0	1	0	±1	Π	2 963.6796
1	0	0	1	0	±1	0	Π	3 169.8195
1	0	0	0	1	0	±1	Π	3 207.7310
0	0	1	2	0	±2	0	Δ	3 433.4153
0	0	1	2	0	0	0	Σ^+	3 433.7196
0	0	1	1	1	1	−1	Σ^+	3 456.4419
0	0	1	1	1	±1	±1	Δ	3 462.6399
0	0	1	1	1	−1	1	Σ^-	3 463.4498
0	2	0	0	0	0	0	Σ^+	3 486.8192
0	0	1	0	2	0	0	Σ^+	3 490.3194
0	0	1	0	2	0	±2	Δ	3 494.8404
1	0	0	2	0	±2	0	Δ	3 663.1512[c]
1	0	0	2	0	0	0	Σ^+	3 663.6756[c]
1	0	0	1	1	1	−1	Σ^+	3 691.9970
1	0	0	1	1	−1	1	Σ^-	3 698.1598
1	0	0	1	1	±1	±1	Δ	3 698.6030
1	0	0	0	2	0	0	Σ^+	3 731.1528
1	0	0	0	2	0	±2	Δ	3 735.8037
0	1	1	0	0	0	0	Σ^+	4 167.4672
0	1	1	1	0	±1	0	Π	4 662.6579
0	1	1	0	1	0	±1	Π	4 700.4866
0	0	2	0	0	0	0	Σ^+	4 834.4642
1	0	1	0	0	0	0	Σ^+	5 064.1724
0	1	1	2	0	0	0	Σ^+	5 162.0874
2	0	0	0	0	0	0	Σ^+	5 334.2740
0	0	2	0	1	0	±1	Π	5 361.0017
1	1	0	1	1	1	−1	Σ^+	5 418.4221
1	0	1	1	0	±1	0	Π	5 549.0692
1	0	1	0	1	0	±1	Π	5 587.5084
2	0	0	0	1	0	±1	Π	5 854.7281
2	0	0	1	1	1	−1	Σ^+	6 324.4484[d]
1	1	1	0	0	0	0	Σ^+	6 780.0709[d]
0	0	3	0	0	0	0	Σ^+	7 207.1658

TABLE IX. (*Continued.*)

v_1	v_2	v_3	v_4	v_5	ℓ_4	ℓ_5	Sym.	G_C^0
1	1	1	1	0	±1	0	Π	7 260.5712[d]
1	1	1	0	1	0	±1	Π	7 304.7744[d]
2	0	1	0	0	0	0	Σ^+	7 674.9864
2	2	1	0	0	0	0	Σ^+	11 058.8678[e]
1	1	3	0	0	0	0	Σ^+	11 431.8487[e]

[a]Upper signs of ℓ_4 or ℓ_5 refer to "e" states; lower signs refer to "f" states. Centre term values, G_C^0, are defined as $G_C^0 = G_v^0 - B_v k^2 - D_v k^4$ (see text).
[b]From Ref. 7.
[c]Not observed experimentally (see text).
[d]From Ref. 11.
[e]From Ref. 10.

The term values of the $\nu_1 + 2\nu_4$ (Σ^+ and Δ) states, which were not observed experimentally, were calculated using the scaled value of the $K^0_{144,155}$ constant in Table III.

Besides the D–D interactions, no other perturbation has been observed in all the analysed bands, with the exception of the Q branch of $2\nu_1 + \nu_5 \leftarrow$ GS, whose transitions show increasing discrepancies between observed and calculated wavenumbers for the "f" levels with $J \geq 24$. This perturbation cannot be ascribed to the 11/33 D–D interaction since the $2\nu_3 + \nu_5 \leftarrow$ GS band is not perturbed and the interaction is also not effective between the $v_1 = 2$ and $v_3 = 2$ states, which are about 500 cm^{-1} apart.

VII. CONCLUSIONS

The IR spectrum of $^{13}C^{12}CD_2$ has been recorded at high-resolution by FTIR spectroscopy from 1800 to 7800 cm^{-1}. The band systems involving the ν_1 and ν_3 stretching excitation and associated ν_4 and ν_5 bending modes have been investigated. In addition, the Q–branch of the ν_1 fundamental was recorded at high resolution using inverse Raman spectroscopy.

In total, 60 cold and hot bands including fundamentals, overtones, stretching–bending, and stretching–stretching combination bands were rotationally analysed. A total of 5881 IR and 35 Raman transitions have been assigned. All transitions involving a given stretching mode were fitted simultaneously to characterize the states with $v_s = 1 (s = 1,2,3)$, $v_s = 2 (s = 1,2,3)$, $v_s = 3 (s = 3)$, and $v_s = v_{s'} = 1$. A set of accurate deperturbed vibration and rotation parameters, including l-type, and D–D interaction constants between $v_4 = 2$ and $v_5 = 2$ levels, has been determined for each stretching mode. Improved sets of parameters for the bending manifolds with $v_{tot} \leq 2$ and for the ν_2 band system have also been obtained using the transitions reported recently.[7,8]

The results of the present investigation complete the characterization of all the vibration modes for the 10 stable isotopologues of acetylene. They provide useful information for the determination of an anharmonic force field and the structure[25] for the molecule based on high precision data for acetylene and its ^{13}C and deuterium substituted isotopologues. In addition, the values of the quartic anharmonic resonance constants can be useful to understand the dynamics of the vibrational energy redistribution and foster further studies on the fully deuterated isotopologues of the molecule.

Tables with the full list of transition wavenumbers, quantum numbers, residuals obtained with the parameters in Tables II–VII, and term values of the levels involved in the transitions, are deposited as supplementary material[26] and are also available from the authors.

ACKNOWLEDGMENTS

The Bologna authors acknowledge the Università di Bologna and the financial support of the Ministero dell' Istruzione dell'Università e della Ricerca (PRIN 2012 "Spettroscopia e Tecniche computazionali per la ricerca Astrofisica, atmosferica e Radioastronomica"). D.B. and R.Z.M. acknowledge the financial support of the Ministry of Economy and Competitiveness through Research Grant No. FIS2012-38175.

[1]Y. Xiao, D. J. Jacob, and S. Turquety, J. Geophys. Res. **112**, D12305, doi:10.1029/2006JD008268 (2007).
[2]A. Coustenis, R. K. Achterberg, B. J. Conrath, D. E. Jennings, A. Marten, D. Gautier, C. A. Nixon, F. M. Flasar, N. A. Teanby, B. Bézard, R. E. Samuelson, R. C. Carlson, E. Lellouch, G. L. Bjoraker, P. N. Romani, F. W. Taylor, P. G. J. Irwin, T. Fouchet, A. Hubert, G. S. Orton, V. G. Kunde, S. Vinatier, J. Mondellini, M. M. Abbas, and R. Courtin, Icarus **189**, 35 (2007).
[3]E. Herbst, Annu. Rev. Phys. Chem. **46**, 27 (1995).
[4]M. Herman, *Handbook of High Resolution Spectroscopy* (John Wiley & Sons, New York, 2011), Vol. 3, pp. 1993–2025.
[5]A. Coustenis, D. E. Jennings, A. Jolly, Y. Bénilanc, C. A. Nixon, S. Vinatier, D. Gautier, G. L. Bjorakerb, P. N. Romani, R. C. Carlson, and F. M. Flasar, Icarus **197**, 539 (2008).
[6]S. Yu, B. J. Drouin, J. C. Pearson, H. M. Pickett, V. Lattanzi, and A. Walters, Astrophys. J. **698**, 2114 (2009).
[7]L. Fusina, E. Canè, F. Tamassia, M. Villa, and G. Di Lonardo, Mol. Phys. **112**, 1123 (2014).
[8]G. Di Lonardo, L. Fusina, A. Baldan, R. Z. Martínez, and D. Bermejo, Mol. Phys. **109**, 2533 (2011).
[9]R. Z. Martínez, J. L. Doménech, D. Bermejo, G. Di Lonardo, and L. Fusina, J. Chem. Phys. **134**, 231102 (2011).
[10]G. Weirauch, M. I. El Idrissi, J. Vander Auwera, M. Herman, and A. Campargue, Mol. Phys. **99**, 969 (2001).
[11]M. Villa, L. Fusina, G. Di Lonardo, X. De Ghellinck d'Elseghem Vaernewijck, and M. Herman, Mol. Phys. **111**, 1972 (2013).
[12]S. Ghersetti, A. Baldacci, S. Giorgianni, R. H. Barnes, and K. Narahari Rao, Gazz. Chim. Ital. **105**, 875 (1975).
[13]D. M. Jonas, S. A. B. Solinas, B. Rajaram, R. J. Silbey, and R. W. Field, J. Chem. Phys. **99**, 7350 (1993).
[14]R. E. Colborn and K. P. C. Vollhardt, J. Labelled Compd. Radiopharm. **20**, 257 (1983).
[15]R. A. Toth, J. Opt. Soc. Am. B **8**, 2236 (1991).
[16]R. A. Toth, J. Opt. Soc. Am. B **10**, 2006 (1993).
[17]G. Guelachvili and K. N. Rao, *Handbook of Infrared Standards II* (Academic Press, Inc., Orlando, Florida, 1986).
[18]G. Guelachvili, M. Birk, Ch. J. Bordé, J. W. Brault, L. R. Brown, B. Carli, A. R. H. Cole, K. M. Evenson, A. Fayt, D. Hausamann, J. W. C. Johns, J. Kauppinen, Q. Kou, A. G. Maki, K. N. Rao, R. A. Toth, W. Urban, A. Valentin, J. Vergès, G. Wagner, M. H. Wappelhorst, J. S. Wells, B. P. Winnewisser, and M. Winnewisser, Pure Appl. Chem. **68**, 193 (1996).
[19]M. Villa, E. Canè, F. Tamassia, G. Di Lonardo, and L. Fusina, J. Chem. Phys. **138**, 134312 (2013).
[20]D. Bermejo, G. Di Lonardo, J. L. Doménech, and L. Fusina, Mol. Phys. **100**(22), 3493 (2002).
[21]D. Bermejo, G. Di Lonardo, J. L. Doménech, and L. Fusina, J. Mol. Spectrosc. **219**, 290 (2003).
[22]D. Bermejo, G. Di Lonardo, J. L. Doménech, and L. Fusina, Mol. Phys. **101**(21), 3203 (2003).
[23]T. R. Huet, M. Herman, and J. W. C. Johns, J. Chem. Phys. **94**(5), 3407 (1990).
[24]E. Canè, G. Cazzoli, G. Di Lonardo, L. Dore, R. Escribano, and L. Fusina, J. Mol. Spectrosc. **216**, 447 (2002).
[25]L. Fusina, E. Canè, F. Tamassia, and G. Di Lonardo, "The experimental equilibrium structure of acetylene" (unpublished).
[26]See supplementary material at http://dx.doi.org/10.1063/1.4929723 for tables of assigned transitions.